Structural Characterization of Biphenyl Ester-Based LC Molecules: Peculiarities of Cyclic Siloxane-Based Materials

T. J. Bunning,*,† H. Korner,‡ V. V. Tsukruk,§ C. M. McHugh,⊥ C. K. Ober,‡ and W. W. Adams⊥

Science Applications International Corporation, 101 Woodman Drive, Dayton, Ohio 45431, Department of Materials Science and Engineering, Bard Hall, Cornell University, Ithaca, New York 14853, College of Engineering and Applied Sciences, Western Michigan University, Kalamazoo, Michigan 49008, and Materials Directorate, Wright Laboratory (WL/MLPJ), Wright-Patterson AFB, Ohio 45433

Received April 30, 1996; Revised Manuscript Received September 30, 1996[⊗]

ABSTRACT: The X-ray meridional profiles of a series of liquid crystalline molecules possessing the same mesogen but different siloxane-based backbones and spacer lengths are compared. Siloxane cores investigated include rings of different sizes, linear polysiloxanes, and short linear segments. The presence of diffuse, periodic reflections for ring-based compounds is attributed in part to translational association of the mesogenic units along the director (strings). The absence of these reflections in smaller, more flexible cores indicates that the localization of strong scattering units induced by the cyclic and linear cores also contributes to the strength of this molecular association. Correlations between measured correlation lengths, orientation parameters, and "string" lengths are discussed in detail. Preliminary molecular modeling is used to investigate the origins of these peculiar scattering phenomena as a function of the molecular architecture.

Introduction

Research into liquid crystalline (LC) systems continues due to their anisotropic optical, electrical, and mechanical properties. Low molar mass liquid crystalline materials have been examined extensively in the development of display technologies.[1−3] Main-chain polymeric LC systems (e.g., Kevlar) have been examined for applications wherein their anisotropy and high strength make them superior to conventional polymeric systems. Side-chain LC systems have also received recent interest for possible uses in passive optical applications including data storage and photonics. Several reviews describing both main-chain and side-chain liquid crystal polymers have been published.[4−6] The structural characterization of these LC systems using X-ray scattering has been discussed in general in many papers reporting on the synthesis and characterization of new LC materials.[7,8]

A class of materials reported on in the past combines the properties of low molar mass LC materials with the glass-forming properties of polymeric systems.[9−11] A subset of this type of material system examined here consists of a central backbone (siloxane-based), onto which are attached various mesogens.[12] Molecular fragments which can be attached possess many properties including liquid crystallinity, photochromism, nonlinear optical behavior, and thermochromism. In past work, real-time diffraction was used to probe the orientation of one such compound consisting of a cyclic siloxane backbone with an attached biphenyl ester-based mesogen under the influence of an applied electric field.[13,14] The ester functionality in the middle of the mesogen promotes a low cross-over frequency in these compounds, allowing switching between parallel and perpendicular alignment with an applied electric field. Coupled with the high flux of a synchrotron, reorientation dynamics between these two types of alignment can be monitored.

Response times, orientation parameters, and correlation lengths as a function of the processing conditions and frequency of the applied field have been examined.[13,14] The scattering patterns from this compound were atypical, as the presence of strong diffuse periodic reflections in the nematic mesophase was observed. The "strength" of these reflections was examined thoroughly by interpreting their occurence as the presence of short-range positional order along the molecular axis. This type of molecular association, termed "strings", has been observed previously in other material systems, namely, small molecules with hydrogen-bonding characteristics and small dimer molecules with nonsymmetric lateral attachment among twin mesogens.[15−17] Some conventional side-chain LC compounds have also exhibited similar diffuse structure, particulary those based on siloxane backbones.[7,18−20]

To examine the effect of small structural differences on this observed atypical scattering behavior,[13,14] compounds with slightly different structures are studied here. Also reported are initial molecular modeling simulations used to explore the molecular origins of this observed association between molecules. The original compound examined was a pentamethylcyclosiloxane ring onto which were attached mesogens based on biphenyl 4-(allyloxy)benzoate (B4AB) mesogens (**I**). This mesogen has $m = 1$, $n = 1$ as shown in Figure 1. Structural variants of this molecule explored in this work include a monomer (**II**) with a slightly longer spacer unit (shorter spacer compounds were not LC), a short linear chain of siloxane units with twin B4AB mesogens (**III**), a linear backbone with B4AB mesogens (**IV**), a tetramethylcyclosiloxane backbone with B4AB mesogens (**V**), and two pentamethylcyclosiloxane-based systems containing biphenyl-based mesogens attached

† Science Applications International Corp.
‡ Cornell University.
§ Western Michigan University.
⊥ Wright-Patterson AFB.
⊗ Abstract published in *Advance ACS Abstracts,* December 1, 1996.

S0024-9297(96)00637-7 CCC: $12.00

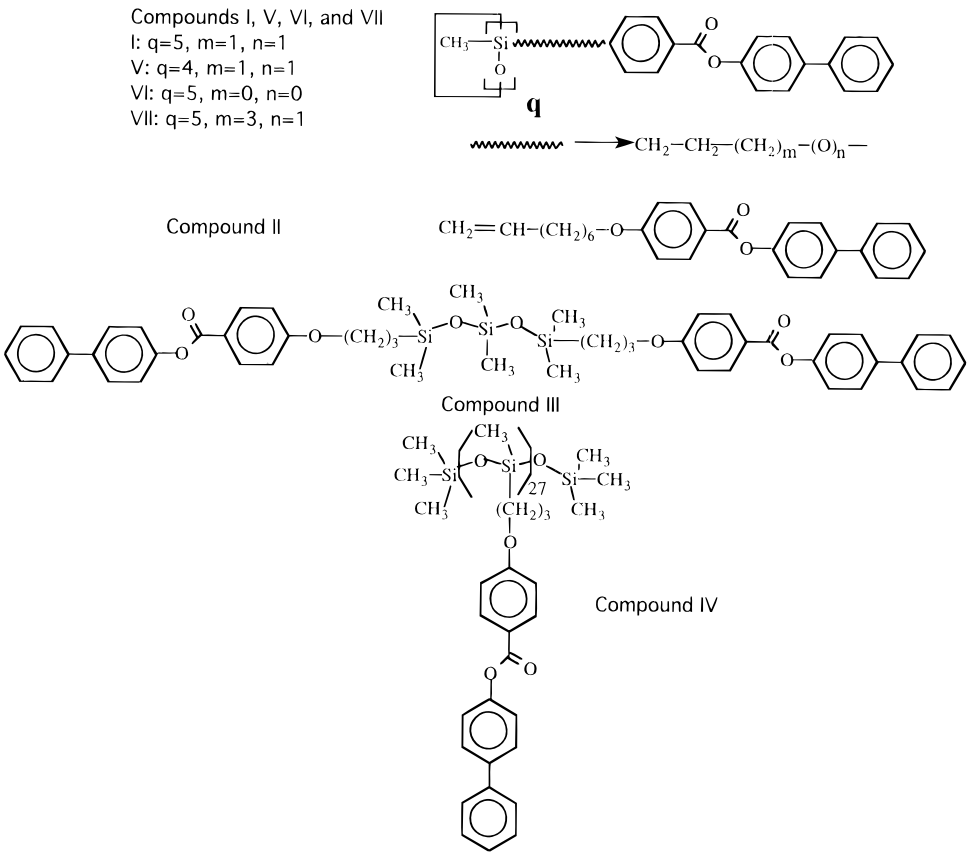

Figure 1. Chemical structures of seven compounds examined. Compounds **I**, **V**, **VI**, and **VII** are ring-based compounds, compound **II** is a model compound of the mesogenic unit common to all compounds, compound **III** is a dimer compound possessing a short chain linear siloxane core capped with two mesogens, and compound **IV** possesses a conventional linear siloxane backbone.

with different length spacer groups (**VI** and **VII**), one shorter and one longer. Figure 1 shows the structure of all compounds, and Table 1 reveals the phase behavior of each. The synthesis and characterization of all compounds have been reported in previous publications.[21,22] In addition, Table 1 lists the reduced temperatures ($T_R = T_{obs}/T_{iso}$) within the nematic phase where aligned diffraction patterns were obtained. All compounds exhibit nematic phases, while **III** and **VII** also exhibit lower temperature smectic phases. The second reduced temperature listed for these two compounds corresponds to alignment in the smectic phase. The reported reduced temperatures represent the lower end of the nematic range. Some of the compounds exhibit narrow nematic temperature ranges, and consequently a high reduced temperature was used. The electric field (e-field) response at two frequencies (10 and 10 000 Hz) is examined in this work. Although the dielectric properties of each compound are a complex function of frequency and temperature, these two frequencies were chosen as they bracket the reorientation behavior previously observed from **I**.[13,14] With the choice of these two frequencies, differences in response indicate how small changes in molecular structure affect the orientation properties.

Experimental Procedures

Alignment procedures in an electric field have been discussed previously.[14] Alignment at a given temperature was performed by heating to the isotropic phase, applying the field, and subsequently cooling to the reported temperature (shown as reduced temperature in Table 1). X-ray data were obtained at the Cornell High Energy Synchrotron Source (CHESS). The detector employed was a CCD detector developed for use at CHESS or image plates, both of which allow a large linear

Table 1. Thermal Transitions on Cooling, *d*-Spacings, and Reduced Temperatures

compound	thermal transitions	*d* (nm)	T_R
I	i 175 n 112 i	2.25	0.88
II	i 131 n 101 k	2.62	0.97
III	i 94 n 89 S_A 64 k	2.56	0.99 or 0.97
IV	i 175 n 55 k	2.22	0.99
V	i 200 n 180 k	2.31	0.97
VI	i 135 n 66 g	none	0.93
VII	i 172 n 140 S_c 120 k	2.47	0.94 or 0.91

intensity range. Wavelengths (λ) used included 1.54, 0.91, and 0.90 Å. Experimental line slice data are reported as intensity as a function of *s* (defined as $2\sin(\Theta)/\lambda$). Samples were probed at approximately 1 V/μm at either 10 or 10 000 Hz. All data analysis from the CCD images was accomplished using a subroutine developed for Matlab which allows for various data manipulations to be performed. Orientation parameters were calculated in a manner similar to those for **I** as have been previously reported.[13,14] Two different approaches are used here to estimate geometrical sizes of ordered regions. First, a classical approach treats the crystal structure as a perfect three-dimensional lattice with limited grain sizes (L_o^*) and uses approximations from general diffraction relationships.[23] The standard Sherrer equation is used to evaluate L_o^* from the fwhm, Δ, of the primary reflection according to the equation[24]

$$L_o^* = k/\Delta s \qquad (1)$$

where Δs is in units of Å^{-1} and *k* is a constant that usually can be considered close to unity.[25] Corrections for instrumental broadening at these scattering angles were insignificant. This approach is reasonable when distortions of molecular packing are low. However, for crystal lattices with significant distortions, application of the Sherrer equation leads to an underestimation of the actual sizes of ordered regions. This

approach can be extended to analyze the size of coherently scattering regions by damping of positional correlations with a characteristic correlation length, ξ. As has been shown for a number of LC and weakly ordered polymers[8,26,27] where damping of positional correlations can be approximated by the Debye exponential equation $G(r) \approx \exp(-r/\xi)$, a simple relationship exists between ξ and the "apparent" geometrical sizes L_0^*, given by

$$L_0^* = (3-4)\,\xi \tag{2}$$

Thus for all compounds, values of ξ are reported corresponding to $L_0^*/3$ evaluated from the fwhm of the primary reflection.

In cases where periodic reflections are present, a second approach can be used to obtain L_s, the "string" length. Estimation of the actual sizes of the crystal lattice, L_s, with distortion of the d-spacings, $g = \delta d/d$, from experimental data can be obtained using a Lorenzian approximation given by the following equation:

$$\Delta s = 1/L_s + \pi^2 g^2 n^2/d \tag{3}$$

where n is the order of the reflection.[25] Plotting Δs versus n^2 allows the intercept ($1/L_s$) and the slope (and thus g) to be obtained. The approach is based on the assumption that the limited sizes of coherently scattered regions are caused by finite sizes of crystal grains with a minor contribution due to distortions. For ideal crystal lattices, $L_0^* = L_s$; for crystals with low distortion ($g = 1-4\%$), $L_0^* < L_s$; and for distorted crystals, $L_0^* \ll L_s$.

Molecular modeling was performed on a Silicon Graphics Power Series workstation using a CERIUS[2] computer simulation package. Energy minimization and molecular dynamics were used to build an isolated molecule with the lowest energy conformation. This molecule was subsequently packed into the crystal unit cell and a crystal lattice minimization was employed for various types of molecular arrangements. We employed mainly orthorhombic primitive and centered unit cells to pack the molecules, although other higher symmetries including trigonal were attempted in some cases. To calculate isotropic ("powder diffraction"), two-dimensional ("fiber diffraction"), and one-dimensional ("meridional scattering") patterns, the Debye formula and the Fourier−Bessel transformation were employed (for further details, see ref 23). Finite sizes of scattering regions, different levels of distortions in various directions, orientational ordering of molecular fragments, and thermal fluctuations all were included in the simulations. These parameters were varied over a wide range to fit the simulation patterns to the experimental scattering curves and the subsequent experimental parameters deduced (crystal sizes, distortion levels, unit cell parameters) from these curves. A detailed description of the modeling procedures along with complete results for some of the LC compounds examined here is discussed in the companion paper.[23] We discuss findings for compounds **II** and **VII** shown in Figure 1, which represent the extremes in experimentally observed complexity.

Results and Discussion

The d-spacings of all compounds ranged between 2.22 and 2.62 nm. In all cases, the d-spacings measured correspond to the length of the biphenyl-based mesogen plus spacer (or tail), with some small contribution due to the siloxane backbone. For **III**, the spacings corresponds to the length of the B4AB unit plus the length of the siloxane unit, indicating full overlap of the molecules. Attachment onto a ring yields slightly larger d-spacings than attachment onto the linear backbone. The average intermolecular distance between mesogenic groups was in the range 0.4−0.6 nm, with lateral correlation lengths in the range 0.5−1.0 nm, typical for short-range lateral ordering of nematic and disordered smectic phases.[28] All compounds except **VII** aligned parallel to the electric field direction at 10 Hz, indicating a positive dielectric anisotropy at this frequency.

Line slices from patterns aligned at 10 Hz along the direction of alignment are shown in Figure 2. Figure 2a shows the strong periodic reflections observed for **I** which prompted this comparison and previous analysis.[13] In general, several (up to five or six) periodic, diffuse reflections can be seen in these meridional scans. Image plates sometimes reveal orders as high as 10. A typical aligned CCD pattern obtained from **V** shows similar diffuse streaks for the smaller ring size compound, as shown in Figure 3. Attachment of the B4AB mesogens to the linear backbone also fosters the appearance of these periodic diffuse reflections, as exhibited by the line slice data for **IV** (Figure 2e). The shorter spacer group **VI** did not align appreciably and did not exhibit the broad small-angle reflection characteristic of a nematic phase (Figure 2g). Compound **VII** exhibited poorly defined multiple reflections along the alignment direction in the nematic phase (Figure 2h). Based on the periodicities of these reflections, these are thought to be the same diffuse reflections observed in **I**, **IV**, and **V**. These reflections were not defined enough to allow further analysis to be undertaken. In addition, the orientation direction for **VII** was orthogonal to the applied field direction, opposite to the rest of the compounds at 10 Hz (Figure 4 versus Figure 3). The large peak in the wide-angle region of the line slice profiles of **III**, **IV**, **VI**, and **VII** is attributed to the lateral distance between molecules and appears due to poor alignment of these compounds. The two small molecules, **II** and **III**, only possess a broad, single diffraction maximum along the alignment direction characteristic of a nematic phase (Figure 2b,c). No indication of the periodic diffuse reflections was present throughout the mesophase range. Compound **II** (Figure 2b) does exhibit additional nonperiodic reflections along the meridian in greatly overexposed images which do not appear on the line slices shown here. Compound **III** (Figure 2c) also shows additional nonperiodic weak reflections along the alignment direction, attributed to weak intramolecular correlations.

The degree of alignment for all of these compounds varied, as indicated by large differences in the orientation parameters shown in Table 2. The correlation length, $\xi_{\parallel}$, obtained from the fwhm of the primary nematic reflection, also varied considerably. The longer spacer group compound **VII** possessed the largest value in the nematic phase, followed by **I**, while the shortest spacer group compound did not exhibit a reflection. This trend reflects the effectiveness of "packing" facilitated by the longer spacer groups. The small change in ring size (**I** versus **V**) also resulted in a large change in the correlation length. However, when comparing data from **V** to those from **I** at a similar reduced temperature, comparable correlation length values are obtained, indicating that similar levels of association are present. The conventional linear siloxane backbone compound **IV** possessed an intermediate correlation length although it exhibited less orientation. Compounds **II** and **III** also showed typical values for correlation lengths among nematics. Both compounds **III** and **VII** exhibit much higher values in the smectic phase, as expected due to the formation of a localized layered structure. The big difference in orientation parameter for **III** in the nematic and smectic regions arises due to the fact that reorientation of the director occurs spontaneously upon its entering the smectic phase. Thus, the director,

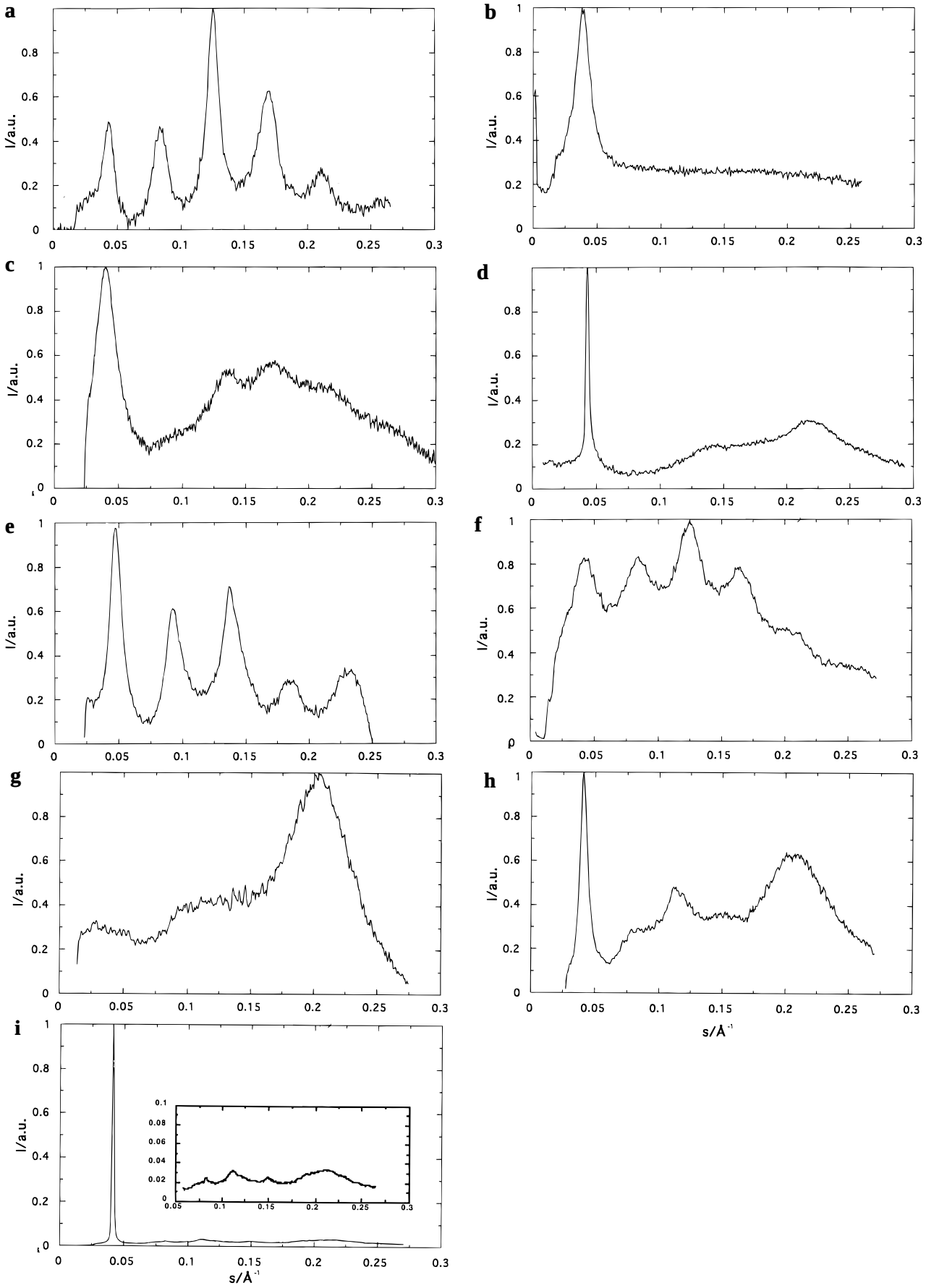

Figure 2. Line slice profiles from the aligned mesophases taken at 10 Hz along the direction of alignment. (a) **I**, (b) **II**, (c) **III** in the nematic phase, (d) **III** in the smectic phase, (e) **IV**, (f) **V**, (g) **VI**, (h) **VII** in the nematic phase, and (i) **VII** in the smectic phase. Note that all scans have been corrected for background scattering, and the strongest intensity has been arbitrarily normalized to 1.

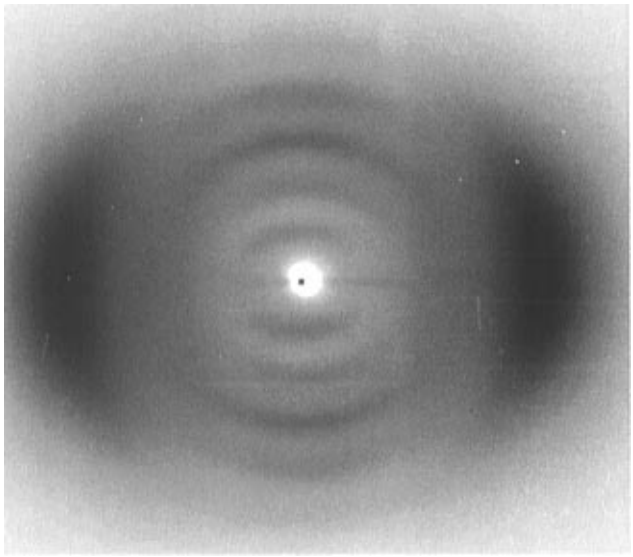

Figure 3. Typical CCD image taken from aligned mesophase showing the appearance of multiple reflections along the alignment direction for **V**. The meridional line slice of this image corresponds to Figure 2f. The electric field direction is vertical.

Table 2. Orientation Parameters, String Lengths, and Correlation Lengths Obtained at 10 Hz at the Reduced Temperatures Shown in Table 1

compound	S_d	L_s (nm)	$\xi_{\parallel}$ (nm)
I	0.55	14.0	4.3
II	0.40	none	2.2
III (nematic)	0.48	none	2.0
III (smectic)	0.15	none	11.6
IV	0.38	8.0	3.1
V	0.62	7.6	2.4
VI	0.19	none	none
VII (nematic)	0.40	nonmeasurable	4.9
VII (smectic)	0.49	nonmeasurable	16.5

initially parallel to the applied field direction, rotates 90° upon entering the smectic phase. This reorientation causes the relatively good alignment to be lost, and subsequent annealing does not improve the resulting orientation.

As the line slice data demonstrate, attachment of these biphenyl-based mesogens to a backbone in general fosters the association responsible for the periodic scattering maxima, with the exception of **VI**, which did not exhibit the small-angle broad reflection characteristic of most nematics. Although some of the intensity distribution may be due to intramolecular correlations, as evidenced by the weak reflections observed for **II** and **III**, the appearance of much stronger reflections for the ring-based compounds is attributed to short-range order along the mesogen direction. Analysis of the width of these reflections versus position gives an indication of the degree of association present (L_s). Compound **I** exhibited the "strongest" strings, corresponding to approximately 5−6 repeat units. Both **IV** and **V** exhibit string lengths of approximately 4 repeat units. Also obtained from this analysis are distortion factors, g, approximately 3−5%. These values are unusually small for common nematic phases, where the range of g values is typically 7−20%.[8] This difference indicates a much lower level of local fluctuations of the spatial positions of cyclic molecules along the main axis as compared to classical nematic phases.

It is interesting to note the lack of correlation between the orientation parameter, the correlation parameter,

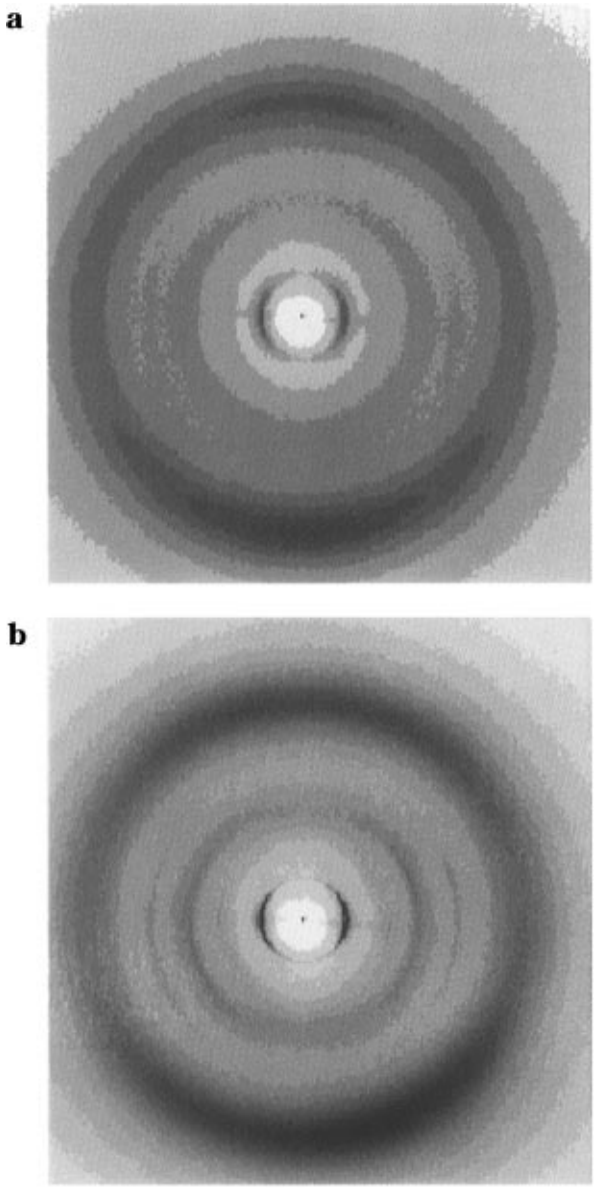

Figure 4. CCD images of **VII** at 10 Hz in the nematic and smectic phases. The alignment direction is orthogonal to that of all other compounds at this frequency relative to the electric field direction (vertical). Line slices (perpendicular to the e-field) from these two images correspond to Figure 2h,i.

and the apppearance of periodic reflections. The largest $\xi_{\parallel}$ value obtained in the nematic phase occurred for **VII**, which did not possess the largest orientation parameter, nor did it exhibit defined periodic reflections. Compound **I** exhibited larger $\xi_{\parallel}$ and L_s values than **V** while possessing a smaller orientation parameter. The poor resolution of the periodic reflections for **VII** is a result of the orthogonal orientation observed for this compound relative to the applied electric field, as shown in Figure 4. This orientation is opposite to that exhibited by all other compounds at 10 Hz. Upon cooling into the smectic phase, the primary reflection of **VII** increases in intensity sharply, as does the correlation parameter, although the definition of the diffuse reflections does not improve. No indication of splitting of the small- or wide-angle reflection is observed, although a smectic-C phase is observed under the microscope. The poor "string" development for this orientation is consistent with examinations of **I** at higher frequencies already reported,[13] wherein a similar orientation was observed. It was shown that the level of association drastically

Table 3. Orientation Parameters, String Lengths, and Correlation Lengths Obtained at 10 000 Hz at the Reduced Temperatures Shown in Table 1

compound	S_d	L_s (nm)	$\xi_{\parallel}$ (nm)
I	0.25	8.9	2.8
IV	0.52	5.6	1.8
V	0.65	7.8	2.4
VII (nematic)	0.71	30	9.3
VII (smectic)	0.67	none	16

decreases when alignment is orthogonal to the field direction.

To further examine the switch to an orthogonal orientation observed previously for **I** at 10 000 Hz, the compounds were examined at the same reduced temperatures at this higher frequency. Previous work attributed this switch in reorientation to a pseudo-Fredericks transition, wherein the sign of the dielectric constant changed from positive to negative.[14] The lower value of the orientation parameter for **I** is a result of this switch in orientation, since a considerable reorientational hindrance of cooperative motion is present. This suggests that the formation of aligned domains is easier than the rearrangement of already aligned domains. Compounds **II**, **III**, and **VI** exhibited behavior similar to that exhibited at 10 Hz at this higher frequency (no differences in orientation and no appreciable differences in the structural parameters listed in Table 2). These values are not listed in Table 3 due to their similarities. Again, it is interesting to note that the orientation parameter and the correlation lengths are not coupled, as **V** exhibits a high degree of alignment (0.65) but a similar level of association compared to **I** while compound **IV** exhibited much lower correlation lengths but a larger orientation parameter.

Compound **VII** showed by far the most dramatic changes in alignment behavior at 10 000 Hz. Not only was the orientation direction opposite that exhibited at 10 Hz in the nematic phase, but a pseudo-Fredericks switching behavior in the nematic phase was observed. Figure 5 shows these strong periodic diffuse reflections in the 2D pattern with the director aligned parallel to the applied field direction. Therefore, a difference in the sign of the anisotropy must be present relative to the same reduced temperature at 10 Hz for this compound. Here, a large orientation parameter was observed in addition to a large correlation length. The magnitude of the correlation length (9.3 nm) at $T_R = 0.94$ is atypical for nematic materials but below that of conventional smectic materials and indicates that this compound lies between a conventional nematic and smectic phase at this temperature. Although the X-ray pattern shown in Figure 5a resembles a smectic pattern, this compound is clearly nematic at this reduced temperature, as evidenced by the characteristic textures observed under an optical microscope. A sharp transition is observed in this texture under the microscope upon cooling slightly into the smectic phase. A texture with disclination loops typical for a nematic phase transforms over a very narrow temperature range into a characteristic focal-conic texture. Coupled with the large value of correlation length, the strong intensity of the first-order reflection observed in the nematic phase (Figure 5a) suggests that a pretransitional smectic structure develops under the influence of the applied field upon cooling from the isotropic phase. A strengthening of the correlation length occurs upon cooling into the smectic phase. A high degree of translational association is also present, as indicated by the large L_s value in the nematic phase. String lengths of approximately 10−12 repeat units in the nematic phase are suggested by the large value of L_s (30 nm).

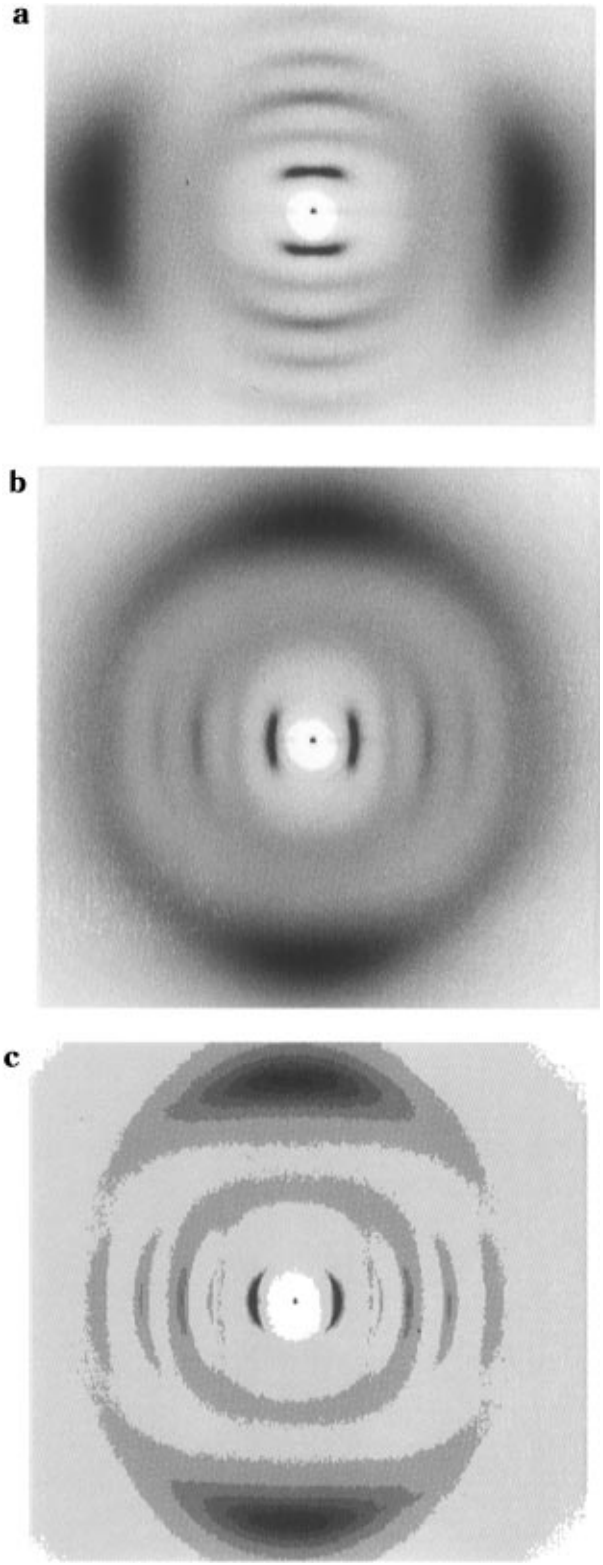

Figure 5. CCD images of **VII** at 10 000 Hz in the nematic phase aligned parallel to the applied field direction (vertical) (a), in the nematic phase aligned orthogonal to the applied field direction caused by a slight decrease in temperature (b), and in the smectic phase upon cooling (c).

Upon cooling close to the nematic−smectic transition at 10 000 Hz, a switch in orientation is observed similar to that exhibited by **I**, as shown in Figure 5b. The director rotates 90° upon cooling from $T_R = 0.94$ to near

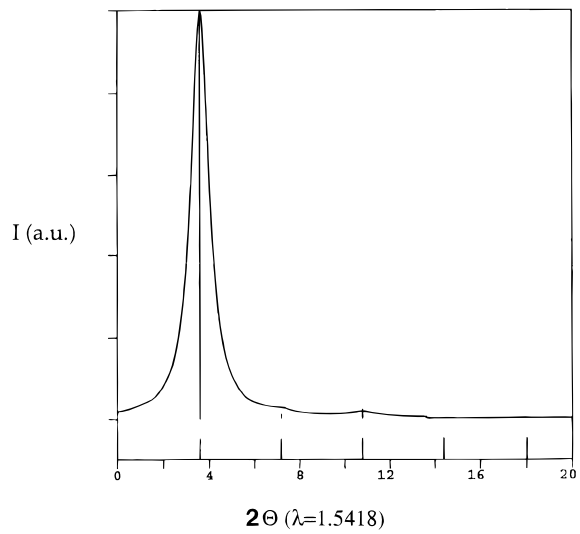

Figure 6. Simulated meridional profile from **II** using a distorted lattice model.

$T_R = 0.93$. Upon further cooling into the smectic phase ($T_R = 0.91$) (Figure 5c), the orientation remains orthogonal to the applied field, and a strong sharpening of the first-order reflection is observed.

To explore the origins of the diffuse periodic scattering patterns reported here, simulated patterns were calculated on **II** and **VII**. Minimization of the total energy of the molecule packed in a *crystal lattice* leads to a primitive orthorhombic cell with parameters $a = 0.62$ nm, $b = 0.38$ nm, and $c = 2.62$ nm. The main axis of the molecule is oriented along the *c*-edge. To fit the simulated X-ray patterns to the experimental data, a lattice factor with very small sizes ($L_{a,b} = 2-3$ nm) and large distortions ($g > \Delta d/d = 10\%$) along the *a*- and *b*-axes was used. The limited sizes of ordered regions and the high level of lattice distortion reflect short-range positional ordering typical for nematic liquid crystals.[8] The best match to the experimental data along the *c*-axis was found using $L_c = 10-15$ nm and $g = 5\%$. The simulated profile shown in Figure 6 compares well to the experimental profile shown in Figure 2b. Therefore, short-range ordering in the *c*-direction of the crystal lattice is expanded over 4−5 molecules. The optimal orientation parameter of molecules used in these simulations was in the range of 0.5−0.6, coinciding with the experimental value (Table 2). Taking into account both experimental uncertainties and the nature of the approach employed, we can conclude that we have reasonably good agreement for "monomeric" **II** without a siloxane ring. The observed X-ray scattering phenomena can be easily interpreted in terms of the formation of a highly *distorted lattice* with a primitive unit cell and short-range ordering of molecules of the nematic type.

Attempts to simulate the complex experimental X-ray scattering of **VII** (diffuse periodic reflections) by packing in a similar distorted lattice to **II** were *not* successful. The centrosymmetric nature of the cyclic molecules packed into a centered orthorhombic unit cell causes an appearance of even ((002), (004), (006), and (008)) orders of reflection along the *c*-axis with periodicities fairly close to those observed experimentally. However, the intensity of the (002) order is an order of magnitude higher than the other reflections, and the (006) reflection constitutes only a small fraction of the total intensity. This result, along with fine details of intensity modulation, contradicts the experimental observations. Therefore, an alternative molecular model was selected to represent the scattering profile along the *c*-direction.

Analysis of the X-ray data indicates that the unusual scattering phenomena observed for **VII** are caused by overlapping of a modulated molecular form factor with strong singularities of the electron density caused by the presence of the siloxane ring with a strong scattering power (equivalent to 40 carbon atoms concentrated within a small volume of about 0.2 nm^3). This contribution is enhanced and modulated by a pseudoregular spatial arrangement of cyclic molecules along the *c*-axis. This kind of molecular association can be related to the previously described string model.[7] We observe, however, that a single string, or head-to-tail packing of molecules in a row along the *c*-direction, does not produce the modulation of meridional scattering observed experimentally.[23] A more complicated association, with correlated arrangement of two rows of cyclic molecules shifted along the *c*-direction (approximately half of the molecular length), produces a distribution of peak intensities close to the experimental observations. An example of the association of three molecules and resulting X-ray meridional scattering is presented in Figure 7a,b. The *d*-spacings of the reflections as well as the relative intensities match those observed experimentally, as shown in Figure 7c. The slight difference in the *d*-spacings (the calculated value is slightly larger than the experimental one) is expected.[23]

The number of molecules simulated along a string was in the range of 2−8. From the calculated meridional scattering patterns, we can estimate the full width at half-maximum, Δs, of each peak. These values can be plotted either versus the length of the string or the squared order of reflection, n^2 (Figure 8a,b). Within experimental accuracy, all fwhms follow the $\Delta s \approx 1/L$ relationship that is very well known for crystalline materials[25] and is the basis for evaluation of crystal sizes in this paper (see $1/L_s$ approximation in Figure 8a). Next, fwhms of all maxima for all lengths of molecular strings follow the well-known rule $\Delta s \approx n^2$ that allows an evaluation of the crystal size (L_s) by extrapolation of Δs to $n = 0$, as has been done for all compounds in this paper (Figure 8b). These results show that the string model simulated here follows general relationships that are well known for partially ordered assemblies.[25]

Figure 8c shows the crystal sizes L_o^* (from fwhm of first maximum) and L_s obtained from the simulated data (Figure 8a,b) for different string lengths. The solid line corresponds to the actual sizes of the molecular string along the *c*-direction. Standard formulas developed for crystal lattices give sizes of ordered regions very close to actual sizes of molecular associations when applied to our simulated model. In addition, this model correctly shows that $L_s > L_o^*$ (defined as above) is valid for partially ordered systems and is consistent with our experimental observations for cyclic LCs. Thus, these results support the applicability of the experimental approaches and quantitative relationships used above for cyclic LCs.

Considering that the experimental value of L_s is approximately 30 nm, from Figure 8c we can estimate the number of repeat units in the correlated string at approximately 10 for **VII** in the nematic phase by extrapolating the line shown in the plot. This means that there are 4−6 cyclic molecules packed in a row along the *c*-direction, with another row of 4−6 molecules

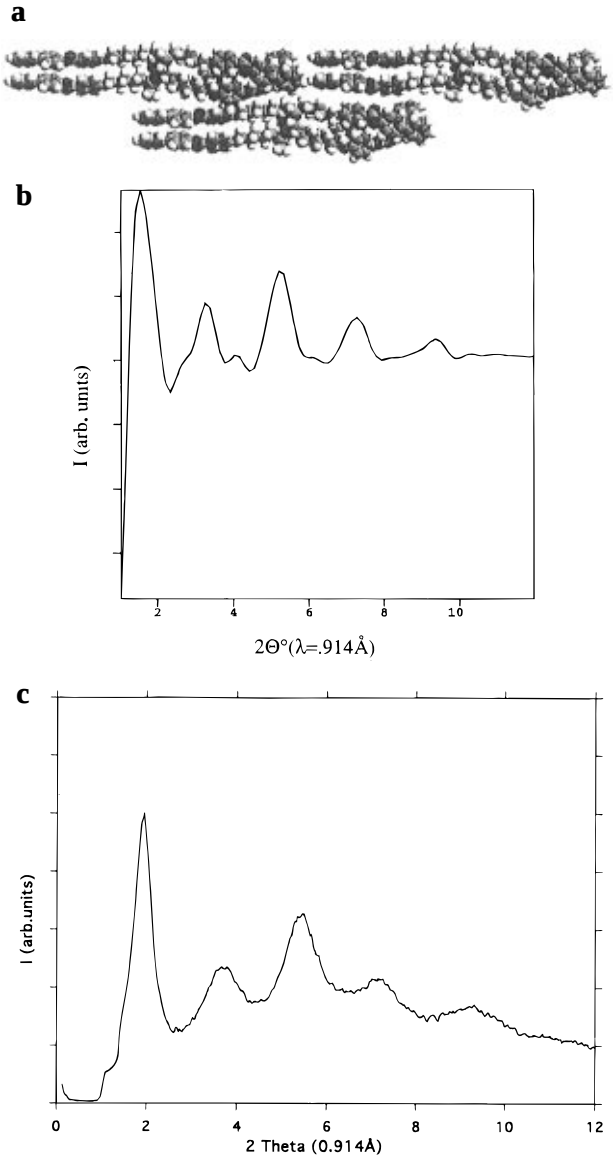

Figure 7. Molecular model of correlated molecular association with three cyclic molecules of **VII** (a), the simulated one-dimensional X-ray scattering pattern (b), and the experimental profile at the high end of the nematic phase (c).

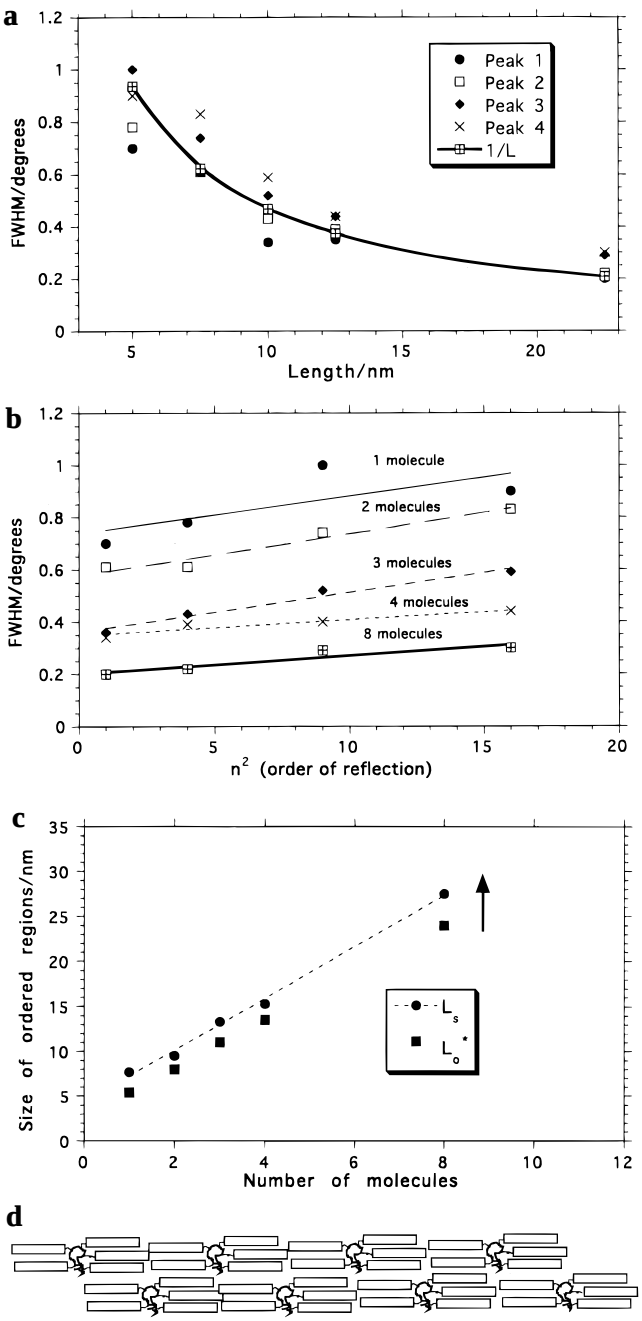

Figure 8. Results from simulated X-ray patterns for molecular strings of **VII** including the variation of fwhm with string length (a), the variation of fwhm with order of reflection (b), crystal sizes deduced from simulated X-ray scattering for various numbers of molecules in a string (c), and a model of the correlated string structure for **VII** (d).

packed side-by-side and shifted approximately a half-molecule (see a sketch of molecular packing for four molecules in the string in Figure 8d). We speculate that this type of association may be enhanced by the specific shape of these cyclic molecules with two and three mesogenic groups on different sides. For this arrangement, a deficit of density on one side and steric limitations on dense packing favor an alternating packing of molecules.

Conclusions

Electric field aligned X-ray diffraction patterns from seven nematic liquid crystalline compounds possessing similar mesogen units with different cores were compared at two frequencies in an electric field. The presence of periodic diffuse reflections parallel to the alignment direction, indicative of atypical molecular association among molecules, was investigated. Two small molecules, one possessing only the mesogen and the other possessing a small linear Si−O segment capped with two mesogens (dimer), showed similar behaviors as only one strong low-angle reflection characteristic of an aligned nematic mesophase was observed. Upon attachment of the same mesogen onto cyclic siloxane cores, periodic diffuse reflections appeared at intensities dependent on the length of the spacer group. The shortest spacer group compound did not reveal any low-angle reflection, while the longest spacer compound shows strong intermolecular association, as evidenced by many meridional reflections. Varying the number of moieties in the cyclic core from 10 to 8 did not appreciably change the level of association observed. A conventional linear polysiloxane-based compound showed intermediate strength meridional diffuse reflections in addition to the characteristic low-angle reflection.

The periodic low-angle diffuse reflections in the X-ray patterns are shown by molecular modeling to be caused by translational association of the mesogenic units along the director ("string"). These simulations indicate that an electron density profile taking into account confined Si−O units is necessary in order for these reflections to occur with similar intensities. Thus, the ring acts to confine the Si−O units to a better degree than the linear backbones based on the relative strength of the periodic reflections. Attachment of the mesogens onto the ring backbones also decreases the local fluctuations of the spatial position of the mesogens along the director as indicated by low distortion factors measured for these cyclic compounds. This "fixing" of the molecules does not occur for the two small molecules, and thus no such association is observed. Lengthening the spacer group allows the mesogens to maximize their tendency to form this string association.

Acknowledgment. T.J.B. acknowledges support through Air Force Contract F33615-95-C-5423. V.V.T. thanks AFOSR for support through the Summer Faculty Research Program and Contract F49620-93-C-0063, and the Petroleum Research Fund, administered by the American Chemical Society. The authors thank David Foti of Matlab for the development of the software analysis package and the Cornell High Energy Synchrotron Source for use of the experimental facilities.

References and Notes

(1) Blinov, L. M. *Electro-optical and Magneto-optical Properties of Liquid Crystals*; John Wiley and Sons: New York, 1983.
(2) Kaneko, E. *Liquid Crystal TV Displays*; KTK Scientific Publishers: Tokyo, 1987.
(3) Drzaic, P. S. *Liquid Crystal Dispersions*; World Scientific: Singapore, 1995.
(4) Donald, A. M.; Windle, A. H. *Liquid Crystalline Polymers*; University Press: Cambridge, 1992.
(5) Plate, N. A., Ed. *Liquid-Crystal Polymers*; Plenum Press: New York, 1993; p 438.
(6) McArdle, C. B., Ed. *Side Chain Liquid Crystal Polymers*; Blackie: Glasgow, 1989; p 448.
(7) Davidson, P.; Levelut, A. M. *Liq. Cryst.* **1992**, *11*, 469.
(8) Tsukruk, V. V.; Shilov, V. V. *Structure of Polymeric Liquid Crystals*; Kiev, 1990.
(9) Shi, H.; Chen, S. H. *Liq. Cryst.* **1995**, *18*, 733.
(10) Shi, H.; Chen, S. H. *Liq. Cryst.* **1994**, *17*, 413.
(11) Kreuzer, F. H.; Andrejewski, D.; Haas, W.; Haberle, N.; Riepl, G.; Spes, R. *Mol. Cryst. Liq. Cryst.* **1991**, *199*, 345.
(12) Bunning, T. J.; Kreuzer, F. H. *Trends. Polym. Sci.* **1995**, *3*, 318.
(13) McNamee, S. G.; Bunning, T. J.; Patnaik, S. S.; McHugh, C. M.; Ober, C. K.; Adams, W. W. *Liq. Cryst.* **1995**, *18*, 787.
(14) McNamee, S. G.; Bunning, T. J.; McHugh, C. M.; Ober, C. K.; Adams, W. W. *Liq. Cryst.* **1994**, *17*, 179.
(15) Wedler, W.; Hartmann, P.; Bakowsky, U.; Diele, S.; Demus, D. *J. Mater. Chem.* **1992**, *2*, 1195.
(16) Deniz, K. U.; Pepy, G.; Keller, P.; Farnoux, B.; Parette, G. *Mol. Cryst. Liq. Cryst.* **1985**, *127*, 81.
(17) Paranjpe, A. S.; Deniz, K. U.; Parvathanathan, P. S.; Amirthalingam, V.; Muralidharan, K. V. *Mol. Cryst. Liq. Cryst.* **1987**, *149*, 79.
(18) Hotz, W.; Strobl, G. *Colloid Polym. Sci.* **1989**, *267*, 889.
(19) Muegge, J.; Zugermaier, P. *Mol. Cryst. Liq. Cryst.* **1988**, *113*, 193.
(20) Lipatov, Y. S.; Tsukruk, V. V.; Shilov, V. V.; Kostromin, S.; Shibaev, V. P. *Polym. Sci. USSR* **1987**, *B29*, 411.
(21) Gresham, K. D.; McHugh, C. M.; Bunning, T. J.; Crane, R. L.; Klei, H. E.; Samulski, E. T. *J. Polym. Sci.: Part A Polym. Chem.* **1994**, *32*, 2039.
(22) Bunning, T. J. Ph.D. Dissertation, University of Connecticut, 1992.
(23) Tsukruk, V. V.; Bunning, T. J.; Korner, H.; Ober, C. K.; Adams, W. W. *Macromolecules* **1996**, *29*, 8706 (preceding paper in this issue).
(24) Alexander, L. E. *X-ray Diffraction Methods in Polymer Science*; Wiley-Interscience: New York, 1969.
(25) Guinier, A. *X-ray Diffraction in Crystals, Imperfect Crystals, and Amorphous Bodies*; Dover Publications: New York, 1994.
(26) Tsukruk, V.; Shilov, V. V. *Sov. Phys. Cryst.* **1988**, *33*, 103.
(27) Tsukruk, V. V.; Shilov, V. V. *Polymer*, **1990**, *31*, 1793.
(28) Tsukruk, V. *Makromol. Chem., Macromol. Symp.* **1991**, *44*, 109.

MA960637W